

Geophysical Research Letters*



RESEARCH LETTER

10.1029/2024GL110379

Key Points:

- Marine heatwaves substantially affect local sea-air CO₂ fluxes via oceanic pCO₂ changes
- During MHWs, tropics decrease outgassing from lower dissolved inorganic carbon, while mid latitudes weaken uptake due to thermally induced rise in oceanic pCO₂
- MHW events can trigger extreme monthly CO₂ flux anomalies, notably in the central equatorial Pacific

Supporting Information:

Supporting Information may be found in the online version of this article.

Correspondence to:

T. L. Frölicher, thomas.froelicher@unibe.ch

Citation:

Li, C., Burger, F. A., Raible, C. C., & Frölicher, T. L. (2024). Observed regional impacts of marine heatwaves on sea-air CO₂ exchange. *Geophysical Research Letters*, 51, e2024GL110379. https://doi.org/10.1029/2024GL110379

Received 23 MAY 2024 Accepted 30 OCT 2024

Author Contributions:

Conceptualization: Friedrich A. Burger, Thomas L. Frölicher

Data curation: Catherine Li Formal analysis: Catherine Li, Friedrich A. Burger

Funding acquisition: Thomas L. Frölicher

Investigation: Catherine Li, Friedrich A. Burger, Christoph C. Raible, Thomas L. Frölicher

Methodology: Catherine Li, Friedrich A. Burger, Christoph C. Raible, Thomas L. Frölicher

Software: Catherine Li, Friedrich A. Burger

Supervision: Friedrich A. Burger, Christoph C. Raible, Thomas L. Frölicher

© 2024. The Author(s).

This is an open access article under the terms of the Creative Commons
Attribution-NonCommercial-NoDerivs
License, which permits use and
distribution in any medium, provided the original work is properly cited, the use is non-commercial and no modifications or adaptations are made.

Observed Regional Impacts of Marine Heatwaves on Sea-Air CO₂ Exchange

Catherine Li^{1,2}, Friedrich A. Burger^{1,2}, Christoph C. Raible^{1,2}, and Thomas L. Frölicher^{1,2}

¹Climate and Environmental Physics, Physics Institute, University of Bern, Bern, Switzerland, ²Oeschger Centre for Climate Change Research, University of Bern, Bern, Switzerland

Abstract Marine heatwaves (MHWs) have devastating effects on ecosystems. Yet a global assessment of the regional impacts of MHWs on the sea-air CO_2 exchange is missing. Here, we analyze 30 global observation-based sea-air CO_2 flux data sets from 1990 to 2019. Globally, the oceanic CO_2 uptake is reduced by 8% (3%–19% across data sets) during MHWs. Regionally, the equatorial Pacific experiences a 31% (3%–49%) reduction in CO_2 release and MHWs often coincide with extreme sea-air CO_2 flux anomalies in this region. The oceanic CO_2 uptake decreases during MHWs by 29% (19%–37%) and 14% (5%–21%) in the low-to-mid latitude Northern and Southern Hemisphere, respectively. Reduced dissolved inorganic carbon in the tropics weakens outgassing, while high ocean temperatures diminish uptake in the low-to-mid latitudes. In the subpolar North Pacific and Southern Ocean, enhanced carbon uptake occurs during MHWs, but uncertainties in pCO_2 data sets limit a comprehensive assessment in these regions.

Plain Language Summary Periods of unusually warm sea surface temperatures (marine heatwaves) have recently been shown to impact the exchange of carbon dioxide (CO₂) between the surface ocean and overlying atmosphere. We find that, on global average, marine heatwaves reduce the oceanic uptake of CO₂ from the atmosphere by 8%. Depending on the region, the local exchange of CO₂ between the ocean and the atmosphere during marine heatwaves can be altered by more than 30%. In tropical regions, the ocean's usual release of CO₂ to the atmosphere is reduced during marine heatwaves due to lower dissolved inorganic carbon in the surface ocean. In low-to-mid latitude regions, the ocean's uptake of CO₂ from the atmosphere is reduced during marine heatwaves due to the effect of warmer temperatures. A clear consensus on the impact of marine heatwaves in the subpolar North Pacific and Southern Ocean does not emerge due to data limitations. While heatwaves in the ocean often coincide with extreme sea-air CO₂ anomalies in the central equatorial Pacific, marine heatwaves are not the main drivers of large temporal variations in monthly sea-air CO₂ exchange outside this region.

1. Introduction

Human-induced carbon dioxide (CO_2) emissions are the primary driver of climate change (IPCC, 2021), with the ocean playing a crucial role in mitigating global warming by taking up about a quarter of these emissions (Friedlingstein et al., 2023). An accurate quantification and understanding of the variability of sea-air CO_2 fluxes is essential for predicting future climate trends (Joos et al., 1999) and assessing the ocean ecosystem response (Gattuso et al., 2015).

In recent decades, prolonged periods of anomalously warm sea surface temperatures, known as marine heatwaves (MHWs; Hobday et al., 2016; Pearce & Feng, 2013), have occurred across all ocean basins (Frölicher & Laufkötter, 2018; Oliver et al., 2021), posing substantial risks to marine species, ecosystems and ecosystem services (Cheung et al., 2021; Cheung & Frölicher, 2020; Collins et al., 2019; Hughes et al., 2017; Smale et al., 2019). With global ocean warming, MHWs are becoming more frequent, intense, and prolonged (Frölicher et al., 2018; Oliver et al., 2018). Individual MHWs are generated by a combination of local oceanic and atmospheric processes including air-sea heat exchange, horizontal and vertical temperature advection, and vertical mixing (Bian et al., 2023; Vogt et al., 2022), and are often associated with large-scale climate phenomena such as the El Niño Southern Oscillation (Holbrook et al., 2019; Oliver et al., 2021).

Recent research has highlighted the significance of MHWs in influencing regional oceanic pCO_2 and sea-air CO_2 fluxes (Arias-Ortiz et al., 2018; Duke et al., 2023; Edwing et al., 2024; Mignot et al., 2022). As one of the first studies, Mignot et al. (2022) identified reduced oceanic CO_2 release in the equatorial Pacific and decreased

LI ET AL. 1 of 12

Validation: Catherine Li
Visualization: Catherine Li, Thomas
L. Frölicher
Writing – original draft: Catherine Li
Writing – review & editing: Friedrich
A. Burger, Christoph C. Raible, Thomas
L. Frölicher

oceanic CO_2 uptake around $40^\circ N$ in the mid-latitude North Pacific during intense and long-lasting MHWs. However, their focus on intense and long-lasting MHWs excludes numerous events and restricts the analysis to specific regions. Duke et al. (2023) examined the North Pacific subpolar gyre, revealing substantial anomalous oceanic CO_2 uptake during recent MHWs due to limited wintertime entrainment and therefore lower oceanic pCO_2 . Additionally, Arias-Ortiz et al. (2018) suggested significant carbon release from seagrass carbon stocks to the atmosphere following the Western Australia 2011 MHW. Despite these insights, a comprehensive global assessment of MHWs impacts on sea-air CO_2 fluxes and their driving mechanisms is lacking. Moreover, understanding if MHWs are the main drivers of extreme sea-air CO_2 anomalies remains limited.

In this study, we explore the impacts of MHW events on sea-air CO_2 exchange at the global scale building on the framework established by Mignot et al. (2022). Using an ensemble of observation-based pCO_2 and wind products spanning from 1990 to 2019, we initially assess the global and regional impacts of MHW events on sea-air CO_2 fluxes. Subsequently, we identify the underlying mechanisms driving flux anomalies during MHWs. Finally, we contextualize these anomalies within the broader spectrum of natural CO_2 flux variability to assess their relative importance in total regional CO_2 flux variability. We extend the scope of the Mignot et al. (2022) study by considering all MHWs instead of a specific subset of persistent MHWs, and use a more comprehensive set of data products for sea-air CO_2 -flux.

2. Methods

2.1. Observation-Based Data

To identify MHWs, we use the global observation-based daily-mean sea surface temperature (SST) data from the National Oceanic and Atmospheric Administration (NOAA; Daily Optimum Interpolation SST OISST dataset v2.1, Huang et al., 2021). This comprehensive data set combines in situ ship and buoy SST observations with satellite-derived measurements from the Advanced Very High-Resolution Radiometer. Through interpolation, data gaps are filled to create a spatially and temporally complete representation of SST. To ensure consistency with the monthly-mean 1° CO₂ flux and oceanic pCO₂ data, the daily mean SST data is regridded from 0.25° × 0.25° to $1^{\circ} \times 1^{\circ}$ and averaged from daily to monthly-mean values, spanning the period 1982 to 2021. This means that shorter-lived small-scale MHWs and their impacts on sea-air CO₂ fluxes are excluded in our analysis. The use of 1° monthly SST data is further by a relatively slow decorrelation time scale of SST anomalies (Hasselmann, 1976). Calculating MHWs using the 1990–2019 instead of the 1982–2019 period does not affect our results (Figure S1 in Supporting Information S1). In addition, the mean sea-air CO₂ flux anomaly during MHWs is largely unaffected by the choice of the SST product. Repeating the analysis with the satellite SST product from the European Space Agency Climate Change Initiative (Merchant et al., 2019), regridded to 1° spatial resolution, shows a similar sea-air CO₂ flux anomaly during MHWs (Figure S2 in Supporting Information S1). Globally, the average anomaly during MHWs differs by only 4%, which is much smaller than the spread in estimates from the CO₂ flux products (Figure 1b).

For the assessment of CO_2 flux anomalies during MHWs, we rely on CO_2 flux estimates derived from the SeaFlux version 2021.04 ensemble data product (Fay et al., 2021). This data set integrates six global observation-based pCO_2 products (Chau et al., 2022; Denvil-Sommer et al., 2019; Gregor et al., 2019; Iida et al., 2020; Landschützer et al., 2014, 2020; Rödenbeck et al., 2013; Zeng et al., 2014), all based on the Surface Ocean Carbon Dioxide Atlas (SOCAT) pCO_2 data set (Bakker et al., 2016), alongside five global wind reanalyzes (Atlas et al., 2011; Hersbach et al., 2020; Kalnay et al., 1996; Kanamitsu et al., 2002; Kobayashi et al., 2015) (Tables S1 and S2 in Supporting Information S1). Combined, we obtain 30 distinct sea-air CO_2 flux data sets at monthly intervals, covering the period 1990 to 2019 on a 1° × 1° grid. We only analyze CO_2 flux data in regions where data from all six observation-based pCO_2 products are available. For example, some observational-based pCO_2 products do not contain data in the northern high latitudes or marginal seas. These regions were omitted in our analysis.

To analyze the drivers of CO_2 flux anomalies during MHWs, we use the LIARv2 alkalinity regression algorithm (Carter et al., 2018). This algorithm utilizes salinity data from the Hadley Center (EN4.2.2; Good et al., 2013) in conjunction with SST data to compute total alkalinity on a $1^{\circ} \times 1^{\circ}$ grid. Dissolved Inorganic Carbon (DIC) is then calculated with CO2SYS (Humphreys et al., 2022) using the estimated total alkalinity, pCO_2 from the six different SeaFlux data products, temperature, salinity, and monthly mean climatologies of phosphate and silicate from the World Atlas 2018 (WOA18; Boyer et al., 2018; Garcia et al., 2019).

LI ET AL. 2 of 12

19448007, 2024, 24, Downloaded from https://agupubs.onlinelibrary.wiley.com/doi/10.1029/2024GL110379 by Universitat Bern, Wiley Online Library on [14/11/2025]. See the Terms

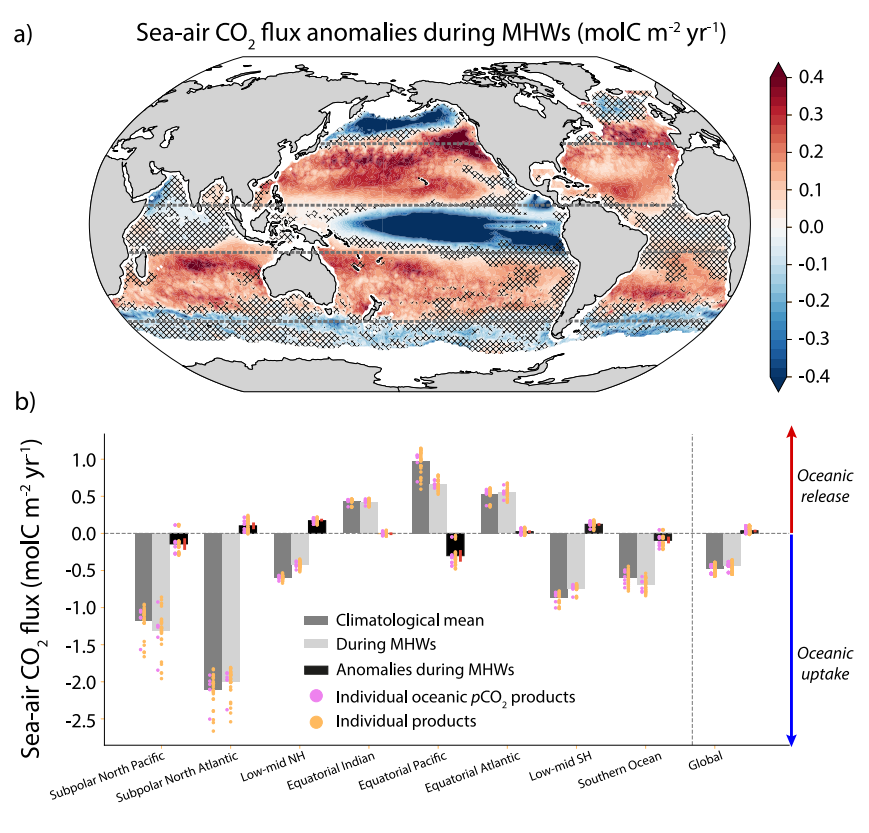


Figure 1. (a) Observation-based sea-air CO_2 flux anomalies during MHWs averaged over the 1990–2019 period and across all observation-based products. Data is only shown for regions where all six observation-based pCO_2 products have data. The gray dashed lines indicate the regions shown in panel (b) and hatching indicate regions, where the anomalies are not statistically different (5% level using a two-sample *t*-test). (b) Climatological mean sea-air CO_2 flux, mean sea-air CO_2 flux during MHWs and mean sea-air CO_2 flux anomalies during MHWs for the years 1990–2019. The bars represent the averages across all observation-based products. The orange points represent the individual 30 observation-based data products. The purple points show the six observation-based pCO_2 products using the average wind product. The red vertical lines indicate the 95% confidence intervals for the mean difference during MHWs obtained from the 30 data products.

2.2. MHW Definition and Sea-Air CO₂ Flux Anomalies

A MHW is identified when the local linearly detrended monthly-mean SST surpasses the local seasonally-varying 90th percentile of SST. The seasonally varying 90th percentile is calculated for each calendar month separately and is based on linearly detrended monthly-mean SST data spanning from 1982 to 2021. The threshold is set to capture extreme temperature anomalies while ensuring a sufficiently large sample size of MHW months for robust statistical analyses. In contrast to the prevailing approach in MHW studies (Hobday et al., 2016; Le Grix et al., 2021), we define MHWs here on monthly anomalies rather than daily anomalies to be consistent with temporal resolution of the CO_2 flux products. We detrended the data to avoid clustering of MHWs toward the end of the time series, due to warming trend in most ocean regions from 1982 to 2019. As oceanic CO_2 uptake increased between 1990 and 2019, clustering would have caused negative anomalies in sea-air CO_2 flux during MHWs, obscuring changes in flux for individual MHWs.

We calculate the monthly mean sea-air CO_2 flux anomalies during MHWs by initially linearly detrending the sea-air CO_2 flux over the period 1990 to 2019. Subsequently, the anomalies during MHWs are derived as deviations from the climatological seasonal cycle of monthly-mean CO_2 fluxes during MHWs.

We divide the global ocean into eight study regions (Figure 1a, and Table S3 in Supporting Information S1) given the diverse characteristics of sea-air CO_2 flux, such as strong or weak oceanic CO_2 sink or source regions. To assess whether the product-ensemble-mean sea-air CO_2 flux during MHWs significantly differs from the mean CO_2 flux (Figure 1), we conduct a standard two-sample *t*-test globally, for each study region, and locally using the

LI ET AL. 3 of 12

5% significance level (Wilks, 2019). To determine the percentile of the mean CO₂ flux during MHWs (Figure 4), we first calculated the local empirical cumulative distribution of all monthly flux anomalies for each grid cell, including both MHW and non-MHW months. The percentile of the CO₂ flux anomaly was identified by locating where the mean flux anomaly during MHWs falls within the local empirical cumulative distribution. This analysis was performed individually for all 30 data products before calculating the average across the data products. We use a one-sample *t*-test with 5% significance level to test whether the product ensemble-mean percentile significantly differs from the 50th percentile, corresponding to no effect of MHWs on sea-air CO₂ flux.

2.3. Decomposition of Sea-Air CO₂ Flux Anomalies Into Drivers

To determine the driving mechanisms behind the sea-air CO_2 flux anomalies during MHWs, we conduct a first-order Taylor series decomposition of the sea-air flux components (Doney et al., 2009; Lovenduski et al., 2007; Mignot et al., 2022; Takahashi et al., 1993). This analysis allows us to quantify the contribution of the solubility, gas transfer velocity, oceanic pCO_2 , and atmospheric pCO_2 to the overall sea-air CO_2 flux anomaly during MHWs.

SeaFlux computes the net sea-air CO_2 flux $(F_{sea-air})$ via the adapted bulk formula established by Wanninkhof (1992):

$$F_{sea-air} = k_w \cdot sol \cdot (pCO_{2,o} - pCO_{2,a}), \tag{1}$$

where k_w is the gas transfer velocity (in units m s⁻¹), *sol* is the solubility of CO₂ in seawater (mol m⁻³ μ atm⁻¹), pCO_{2,o} is the partial pressure of surface ocean CO₂ (μ atm) and pCO_{2,o} represents the partial pressure of atmospheric CO₂ in the marine boundary layer (μ atm). Note that the bulk formula is adapted to omit sea ice regions as not all data products encompass these regions.

The first order Taylor series decomposition of the sea-air CO_2 flux anomalies during MHWs (referred to hereafter as $\Delta F_{sea-air}$) is as follows:

$$\Delta F_{\text{sea-air}} \approx \underbrace{\frac{\partial F_{\text{sea-air}}}{\partial k_{\text{w}}} \cdot \Delta_{k_{\text{w}}}}_{k_{\text{w}} \text{ contribution}} + \underbrace{\frac{\partial F_{\text{sea-air}}}{\partial sol} \cdot \Delta_{sol}}_{sol \text{ contribution}} + \underbrace{\frac{\partial F_{\text{sea-air}}}{\partial \text{pCO}_{2,\text{o}}} \cdot \Delta_{\text{pCO}_{2,\text{o}}}}_{\text{pCO}_{2,\text{o}} \text{ contribution}}$$

$$+ \underbrace{\frac{\partial F_{\text{sea-air}}}{\partial \text{pCO}_{2,\text{a}}} \cdot \Delta_{\text{pCO}_{2,\text{a}}}}_{\text{pCO}_{2,\text{contribution}}}$$
(2)

The right hand side of Equation 2 represents the contributions of the gas transfer velocity, solubility, and oceanic and atmospheric partial pressure of CO_2 . The delta values represent the mean anomalies of the variables during MHWs and the partial derivatives are calculated with the temporal mean values.

The oceanic pCO_2 anomalies are further decomposed as:

$$\Delta \text{pCO}_{2,o} \approx \underbrace{\frac{\partial \text{pCO}_{2,o}}{\partial \text{DIC}} \cdot \Delta_{\text{DIC}}}_{p\text{CO}_{2,o}^{\text{DIC}}} + \underbrace{\frac{\partial \text{pCO}_{2,o}}{\partial \text{ALK}} \cdot \Delta_{\text{ALK}}}_{\text{pCO}_{2,o}^{\text{ALK}}} + \underbrace{\frac{\partial \text{pCO}_{2,o}}{\partial T} \cdot \Delta_{T}}_{\text{pCO}_{2,o}^{T}} \cdot \Delta_{T} + \underbrace{\frac{\partial \text{pCO}_{2,o}}{\partial S} \cdot \Delta_{S}}_{\text{pCO}_{2,o}^{S} \text{ contribution}}$$
(3)

where oceanic $pCO_{2,o}$ is a function of sea surface DIC, alkalinity (ALK), temperature (T), and salinity (S). The 'mocsy 2.0' Fortran 95 routine (Orr & Epitalon, 2015) is used to calculate the partial derivatives, evaluated at temporal mean values for S, T, DIC, ALK, phosphate, and silicate.

3. Results

3.1. Global and Regional Response of Sea-Air CO₂ Fluxes During MHWs

Globally, the oceanic uptake of CO_2 is reduced by an average of 0.04 mol C m⁻² yr⁻¹ during MHWs (confidence interval: 0.02–0.05 mol C m⁻² yr⁻¹), with values ranging from -0.01 (anomalous uptake) to 0.11 mol C m⁻² yr⁻¹ (anomalous release) depending on the data set used (Figure 1b). This corresponds to an 8% (range: 3%–19%)

LI ET AL. 4 of 12

reduction in oceanic uptake of CO_2 averaged over all MHWs over the time period from 1990 to 2019. In 48% of the ocean surface area covered by the CO_2 flux products, the CO_2 flux - whether into or out of the ocean in the climatological mean - is weakened during MHWs (Figure S3 in Supporting Information S1). In 8% of the area, the flux is enhanced, while in 44% of the area, the changes are statistically insignificant.

Regionally, the CO_2 uptake is reduced during MHWs by an average of 0.10 (range: -0.01 to 0.24; confidence interval of mean: 0.07 to 0.13) mol C m⁻² yr⁻¹ in the subpolar North Atlantic, 0.17 (range: 0.11–0.22; confidence interval: 0.16 to 0.18) mol C m⁻² yr⁻¹ in the low-to-mid latitude Northern Hemisphere and 0.12 (range: 0.04 to 0.18; confidence interval: 0.11 to 0.14) mol C m⁻² yr⁻¹ in the low-to-mid latitude Southern Hemisphere. This corresponds to reductions of 5% (range: 0%–12%) in the subpolar North Atlantic, 29% (range: 19%–37%) in the low-to-mid latitude Northern Hemisphere, and 14% (range: 5%–21%) in the low-to-mid latitude Southern Hemisphere. In the equatorial Pacific, CO_2 outgassing decreases by an average of 0.30 (range: -0.03 to 0.48; confidence interval: 0.25 to 0.35) mol C m⁻² yr⁻¹, which corresponds to a 31% (range: -3 to 49%) reduction. In contrast, the subpolar North Pacific shows an increase of CO_2 uptake by 0.14 (range: -0.12 to 0.30; confidence interval: 0.09 to 0.19) mol C m⁻² yr⁻¹, corresponding to a 12% (range: -10% to 25%) increase during MHWs. Similarly, in the Southern Ocean, the CO_2 uptake is 0.09 (range: -0.05 to 0.22; confidence interval: 0.06 to 0.12) mol C m⁻² yr⁻¹ or 15% (-9 to 36%) stronger during MHWs.

The spread in the sea-air CO_2 flux anomalies during MHWs across all observation-based products is considerable (Figure 1b). The primary contributors to this spread are the pCO_2 data sets, as indicated by the contrast between the purple and orange dot ranges in Figure 1b. Minimal variation is observed between CO_2 flux anomalies calculated with the average pCO_2 product and different wind products (not shown), further underscoring the role of pCO_2 reconstructions as the primary source of uncertainty. As a result, significant regionally averaged CO_2 flux anomalies during MHWs are only detectable in four of the eight study regions (5% level using a two-sample t-test): the equatorial Pacific, the low-to-mid latitudes in both hemispheres, and the Southern Ocean. While statistical significant changes are observed in the Southern Ocean, a comprehensive assessment is hindered by the absence of the pCO_2 data, particularly during austral winter (Gray et al., 2018; Landschützer et al., 2016). Locally, significant changes are also observed in parts of the Subpolar North Pacific and North Atlantic (Figure 1a). However, such significant changes are largely absent in the tropical Indian and Atlantic Ocean.

3.2. Drivers of Sea-Air CO₂ Flux Changes During MHWs

To quantify the drivers of sea-air CO_2 flux changes during MHWs, we apply the Taylor decomposition to all sea-air flux components (gas transfer velocity, solubility, oceanic and atmospheric pCO_2 ; Equation 2). Oceanic $pCO_{2,0}$ changes emerge as the primary driver of sea-air CO_2 flux anomalies during MHWs in most regions (Figure 2; Figure S4 in Supporting Information S1). Notably, regions such as the subpolar North Pacific (Figure 2b), the equatorial Pacific (Figure 2f) and the Southern Ocean (Figure 2i) experience anomalously lower oceanic $pCO_{2,0}$ (i.e., a negative $pCO_{2,0}$ contribution), leading to decreased sea-air CO_2 fluxes during MHWs. Conversely, the low-to-mid latitudes in both hemisphere (Figures 2d and 2h) experience higher oceanic $pCO_{2,0}$ (i.e., a positive $pCO_{2,0}$ contribution) and therefore higher sea-air CO_2 fluxes during MHWs. In the northern Indian Ocean and parts of the North Atlantic and Southern Ocean, weaker gas transfer velocities during MHWs (i.e., weaker winds) are the primary driver of sea-air CO_2 flux anomalies.

The secondary driver of sea-air CO_2 flux anomalies varies across regions. In the equatorial Pacific (Figure 2f), anomalous CO_2 uptake is also substantially driven by weaker gas transfer velocities during MHWs. In the subpolar North Pacific (Figure 2b), reduced solubility and weaker gas transfer velocities somewhat offset the stronger uptake. In the subpolar North Atlantic (Figure 2c), the anomalous outgassing is caused by a combination of weaker gas transfer velocities and lower solubility, which reduce the region's ability to uptake CO_2 and outweigh the decrease in $pCO_{2,0}$ observed during MHWs. In the equatorial Indian (Figure 2e) and Atlantic Ocean (Figure 2g), the very small CO_2 flux anomalies during MHWs are a result of small and counterbalancing contributions of changes in oceanic $pCO_{2,0}$ and the gas transfer velocities. The atmospheric $pCO_{2,a}$ changes play a negligible role in all regions, except in parts of the Southern Ocean and the tropical ocean.

By breaking down the oceanic $pCO_{2,0}$ anomalies during MHWs (Equation 3), we can attribute the flux response to a balance between thermal (temperature) and non-thermal DIC effects on oceanic $pCO_{2,0}$ (Figure 3), along with changes in alkalinity and salinity. In all ocean regions, the thermal effect - resulting from elevated sea surface

LI ET AL. 5 of 12

19448007, 2024, 24, Downloaded from https://agupubs.onlinelibrary.wiley.com/doi/10.1029/2024GL110379 by Universitat Bern, Wiley Online Library on [14/11/2025]. See the Terms and Conditions (https://onlinelibrary.wiley

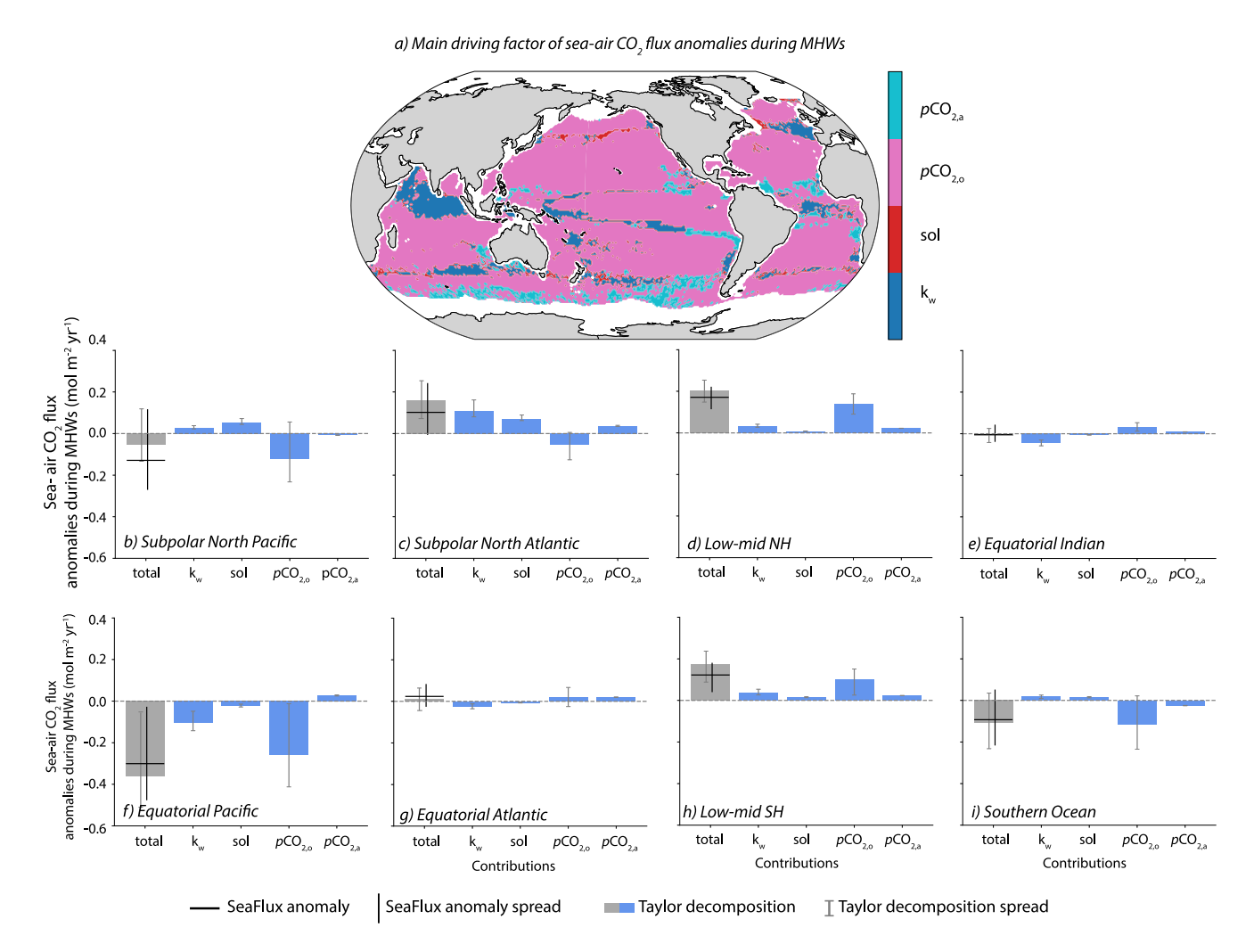


Figure 2. Local dominant and regional drivers of sea-air CO₂ flux anomalies during MHWs over the 1990–2019 period across all observation-based products. The dominant driver in each grid cell is shown in panel (a). The blue bars in panels (b–i) represent the average contribution of each flux term to the sea-air CO₂ flux anomalies during MHWs with gray error bars representing the min-max spread across the 30 observation-based data products. The gray bar is the sum of all the contribution terms. For comparison, the horizontal black line is the averaged observation-based product sea-air CO₂ flux anomalies during MHWs, and the black error lines represent the min-max spread across the 30 observation-based data products. A positive contribution indicates anomalous outgassing, while a negative contribution suggests anomalous uptake. The results are shown for regions where all six observation-based CO₂ flux products have data.

temperatures during MHWs - positively contributes to oceanic $pCO_{2,0}$ anomalies. This is due to the decrease in CO_2 solubility in seawater and due to an increase in CO_2 concentration from a shift in chemical equilibrium between carbonate species with rising temperatures, both leading to anomalously higher oceanic $pCO_{2,0}$. Simultaneously, lower DIC concentrations during MHWs result in anomalously lower oceanic $pCO_{2,0}$ in all ocean regions. The dominance of either the temperature or DIC effect varies by region (Figure 3; Figure S5 in Supporting Information S1). In the equatorial Pacific (Figure 3f) and high latitude regions like the subpolar North Pacific (Figure 3b), subpolar North Atlantic (Figure 3c), and Southern Ocean (Figure 3i), the decrease in oceanic $pCO_{2,0}$ anomalies driven by DIC outweighs the increase caused by thermal effects. This DIC-driven effect is particularly notable in the equatorial Pacific, where it counteracts both thermal and alkalinity-driven $pCO_{2,0}$ increases during MHWs, resulting in lower than usual $pCO_{2,0}$ (-8.43 (-12.40 to 0.25) μ atm) and reduced outgassing fluxes. In contrast, in low-to-mid latitude regions (Figures 3d–3h), the thermal-driven increase in oceanic $pCO_{2,0}$ typically dominates the flux response during MHWs. In regions where the thermal effect compensates the DIC effect, such as in the Indian Ocean or tropical Atlantic, the sea-air CO_2 flux anomalies are often not statistically significant (Figure 1a). Changes in alkalinity play a moderate role in the equatorial Pacific (Figure 3f)

LI ET AL. 6 of 12

19448007, 2024, 24, Downloaded from https://agupubs.onlinelibrary.wiley.com/doi/10.1029/2024GL110379 by Universitat Bern, Wiley Online Library on [14/11/2025]. See the Terms and Conditions (https://online

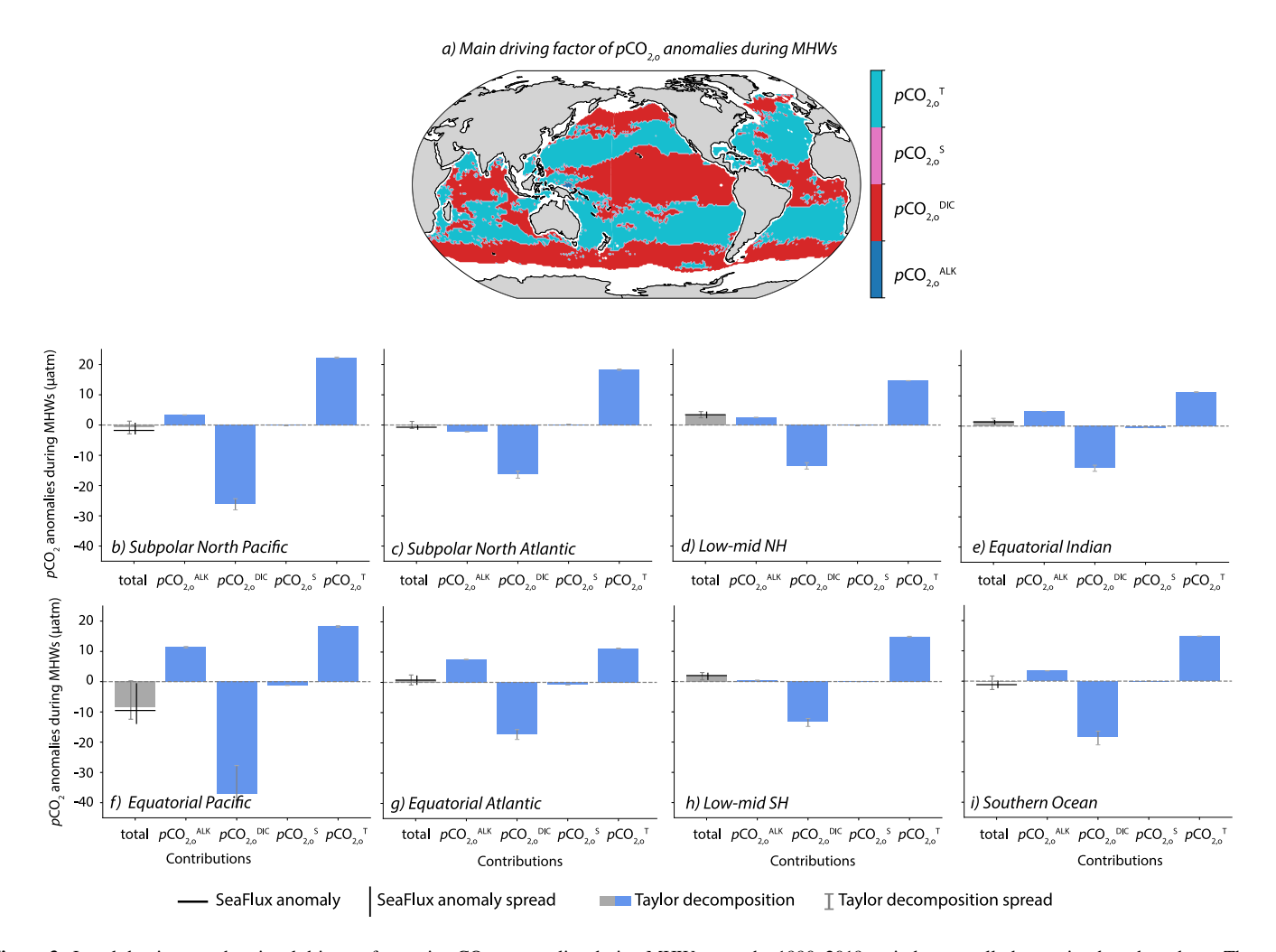


Figure 3. Local dominant and regional drivers of oceanic $pCO_{2,0}$ anomalies during MHWs over the 1990–2019 period across all observation-based products. The dominant driver in each grid cell is shown in panel (a). The blue bars in panels (b–i) represent the average contribution of each $pCO_{2,0}$ term to the total $pCO_{2,0}$ anomalies during MHWs with gray error bars representing the min-max spread across the 30 observation-based data products. The gray bar is the sum of all the contribution terms. For comparison, the horizontal black line is the averaged observation-based product oceanic $pCO_{2,0}$ anomalies during MHWs, and the black error lines represent the min-max spread across the 30 observation-based data products. A positive total contribution indicates an increase in oceanic $pCO_{2,0}$. The results are shown for regions where all six observation-based $pCO_{2,0}$ products have data.

and equatorial Atlantic (Figure 3g). However, in all other regions, both alkalinity and salinity changes play a negligible role. Using the OceanSODA-ETHZ alkalinity data from Gregor and Gruber (2021) instead of the alkalinity data based on LIARv2 yields similar results (Figure S6 in Supporting Information S1).

It is important to note that a potential limitation of the Taylor decomposition is the assumption of linearity as we know that the functions governing sea-air CO_2 flux are non-linear. To check whether this limitation has an impact on our attribution of the drivers we compare the sum of the Taylor decomposition terms with the calculated flux and driver anomalies. In particular for the sea-air CO_2 flux changes (gray bar vs. horizontal black lines in Figures 2 and 3), there are slight discrepancies: the Taylor decomposition tends to overestimate the flux anomalies in the subpolar North Atlantic (Figure 2b), equatorial Pacific (Figure 2f) and low-to-mid latitudes (Figures 2d–2h), while underestimating anomalies in the subpolar North Pacific (Figure 2b). Thus, this limitation may alter our quantitative assessment of the drivers, but we maintain confidence in the robustness of the qualitative findings of the drivers.

LI ET AL. 7 of 12

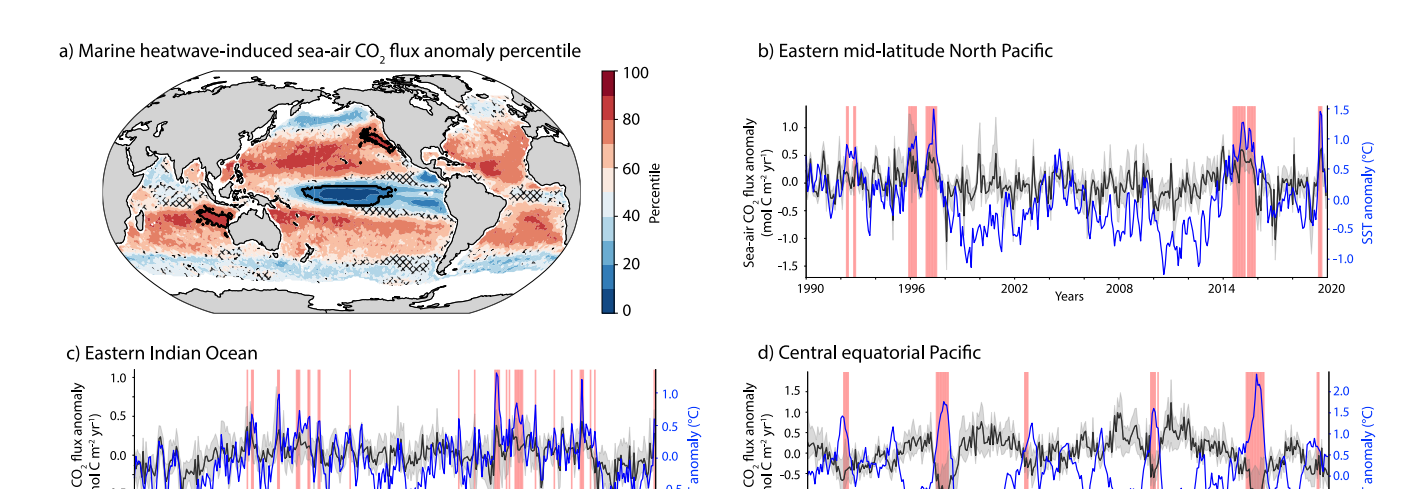


Figure 4. (a) Global pattern of the percentile associated with the mean sea-air CO₂ flux anomalies averaged over all MHW months, compared to the local empirical distribution of monthly detrended sea-air CO₂ flux anomalies from 1990 to 2019. Hatching indicates regions, where the mean percentiles are not significantly different from the 50th percentile (i.e., representing no effect of MHWs on air-sea CO₂ flux; 5% level using a one-sample *t*-test). (b–d) For three specific illustrative regions (highlighted in panel a as black contours), the time series of the mean monthly detrended sea-air CO₂ flux anomalies across all data products, detrended sea surface temperature anomalies (blue lines) and identified MHW events (red shading) are shown. The black shading in b-d shows the min-max range across all 30 sea-air CO₂ flux data products.

3.3. Importance of MHW-Induced CO₂ Flux Anomalies Within Its Natural Variability

Next, we examine the importance of CO₂ flux anomalies induced by MHWs in the broader context of natural variations in sea-air CO₂ exchange. Our aim is to determine whether strong CO₂ flux anomalies primarily coincide with MHWs or if MHWs play a relatively minor role in explaining the variations in sea-air CO₂ fluxes.

Across much of the global ocean, the mean sea-air CO_2 flux anomalies during MHWs remain within the 90% or 10% percentile of typical background flux variations (Figure 4a). This suggests that MHWs do not often coincide with extreme anomalies in sea-air CO_2 fluxes. However, the central equatorial Pacific stands out with a pronounced CO_2 flux response during MHWs, where mean CO_2 flux anomalies drop below the tenth percentile of the flux distribution (Figures 4a and 4d). In this region, MHWs often coincide with low sea-air CO_2 flux events as shown with a high likelihood multiplication factor (Le Grix et al., 2021; Zscheischler & Seneviratne, 2017) in Figure S7 in Supporting Information S1. The periods of extreme anomalous CO_2 uptake in the central equatorial Pacific often coincide with El Niño events in these regions (Holbrook et al., 2019; Le Grix et al., 2021; Oliver et al., 2019). For example, the strongest El Niño events in 2015/2016 and of 1997/98 align with the most extreme anomalous oceanic CO_2 uptake observed in the past 30 years in this region.

We further explore the temporal evolution of CO₂ flux anomalies in the eastern Indian Ocean and eastern North Pacific, where individual MHWs have strongly impacted marine ecosystems (and sea-air CO₂ fluxes) in the past two decades. In the eastern North Pacific (Figure 4b), strong outgassing events also often coincide with MHWs, especially earlier in the period, though the variability between data products remains high. In the eastern Indian Ocean (Figure 4c), particularly off the northwest coast of Australia, MHWs triggered extreme anomalous CO₂ outgassing in 2010/11 and 2015/16.

4. Discussion and Conclusions

We show that the global oceanic uptake of CO_2 is reduced during MHWs by about 8%. Regionally, MHWs diminsh the sea-air CO_2 fluxes by up to 30%, such as in the equatorial Pacific and the low-to-mid latitude region of the Northern Hemisphere. We find the flux responses to be mainly driven by changes in the partial pressure of CO_2 in the ocean, which are a net result of two competing mechanisms during MHWs: a thermal effect and a non-thermal DIC effect. In regions where decreases in oceanic $pCO_{2,0}$ reduce CO_2 outgassing (e.g., equatorial Pacific)

LI ET AL. 8 of 12

or increase CO_2 uptake (subpolar North Pacific and Southern Ocean), the primary driver is a reduction in DIC. In contrast, in regions (e.g., mid-latitudes) where increases in oceanic $pCO_{2,0}$ diminish the oceanic CO_2 uptake, temperature rises are the main driving factor for changes in oceanic $pCO_{2,0}$.

Our results align with Mignot et al. (2022) in the equatorial Pacific, where DIC outweighs the temperature effect on oceanic $pCO_{2,0}$, resulting in a comparable reduction in outgassing (31% reduction in our study vs. 40% decrease in Mignot et al. (2022)). The agreement is not surprising given that the analysis here is based on similar (though more) $pCO_{2,0}$ products as used in Mignot et al. (2022). Additionally, the additional constraint of focusing on 'persistent' MHWs in Mignot et al. (2022) is not needed in this region, since long-lasting El Niño driven MHW are prevalent there (Holbrook et al., 2019).

Our results suggest that the findings of Mignot et al. (2022) regarding anomalous outgassing in the mid-latitude North Pacific during MHWs, attributed to thermal effect dominating over the DIC effect, can be extrapolated to low-to-mid latitude CO_2 uptake regions in both hemispheres. However, whether alterations to the horizontal advection are the main drivers of the DIC decrease in the low-to-mid latitude regions, as shown for the North Pacific by Mignot et al. (2022), remains an open question.

In the high latitudes, MHWs induce different sea-air CO_2 flux responses, with regions such as the Southern Ocean and subpolar North Pacific experiencing enhanced carbon uptake, while others like the subpolar North Atlantic show attenuated uptake. Nevertheless, the findings of this study suggest that in high latitudes, the $pCO_{2,0}$ response during MHWs is primarily driven by the non-thermal DIC effect. Furthermore, this DIC-driven $pCO_{2,0}$ response controls the flux response in the Southern Ocean and the subpolar North Pacific, consistent with Duke et al. (2023).

The general compensating nature of the thermal and non-thermal DIC effects on $pCO_{2,0}$, as already discussed in Mignot et al. (2022), was also identified in Burger et al. (2022), where the response in hydrogen ion concentration ([H+]) and $pCO_{2,0}$ during MHWs was analyzed. The response of $pCO_{2,0}$ during MHWs also resembles seasonal variations in $pCO_{2,0}$. In low-to-mid latitudes, the thermally driven increase in oceanic $pCO_{2,0}$ during summertime is slightly counteracted by the decrease in oceanic $pCO_{2,0}$ due to increased stratification which brings less DIC to the surface, but ultimately the thermal effect prevails. In contrast in high latitudes, the seasonal variations in $pCO_{2,0}$ are controlled by DIC, with decreases in DIC during summer reducing $pCO_{2,0}$ despite thermally driven increases in $pCO_{2,0}$ (Fay & McKinley, 2017; Takahashi et al., 2002).

Our study shows that MHWs in certain ocean regions, such as in Western Australia (e.g., in 2011; Arias-Ortiz et al. (2018)) or the central tropical Pacific can coincide with extreme CO_2 flux anomalies. However, such extreme CO_2 flux anomalies during MHWs are more exceptional than common in the global. This is in contrast to the often extreme impact of land heat waves on terrestrial carbon fluxes, driven by factors such as soil moisture deficits, heat stress, and increased fire activity (Frank et al., 2015; Reichstein et al., 2013). For example, the summer 2003 heatwave and drought event in Europe reduced gross primary production by about 30% (Ciais et al., 2005), and the global heatwave in 2023 possibly reduced global land CO_2 uptake by 78% (0.44 \pm 0.21 GtC yr⁻¹ in 2023, compared to an average of 2.04 GtC yr⁻¹ in the period 2010–2022; (Ke et al., 2024)). These anomalies are substantially larger than the normal variability.

Furthermore, we show that observation-based products generally agree with each other regarding the direction of sea-air CO_2 flux anomalies during MHWs in the low-to-mid latitudes and the equatorial Pacific. However, discrepancies arise in higher latitudes, notably the subpolar North Pacific and Southern Ocean, possibly due to limited observational data in these regions. The lack of comprehensive data underscores the need for improved observation-based data sets and sustained data collection (Dong et al., 2024). Such data, preferably in higher spatial and temporal resolution than used in our current study, will enable us to enhance our understanding of how sea-air CO_2 fluxes respond to climate extremes, particularly in crucial carbon sink areas. Moreover, future research should investigate the seasonal influence on the sea-air CO_2 flux response to MHWs, as the dominant effect on oceanic $pCO_{2,0}$ (thermal vs. non-thermal) may vary by season (Burger & Frölicher, 2023). In addition, the sea-air CO_2 flux response to MHWs under future climate conditions should be explored, as changes in stratification, ocean carbon content, biological production and wind patterns may impact this response.

LI ET AL. 9 of 12

Data Availability Statement

The NOAA OISSTv2.1 data is available under https://www.ncei.noaa.gov/products/optimum-interpolation-sst, the Hadley Centre EN4.2.2 salinity data under https://www.metoffice.gov.uk/hadobs/en4/download-en4-2-2. html, the phosphate and silicate World Atlas 2018 data under https://www.ncei.noaa.gov/access/world-ocean-atlas-2018/, the OceanSODA-ETHZ Alkalinity data under https://doi.org/10.25921/m5wx-ja34, and the ESA-C3S SST data under https://doi.org/10.48670/moi-00169. The analysis scripts as well as the carbonate chemistry data sets based on the SeaFlux pCO_2 that are used for Figure 3 and Figures S5 and S6 in Supporting Information S1 are available under Zenodo (Li & Burger, 2024).

Acknowledgments

This work has received funding from the Swiss National Science Foundation (PP00P2 198897) the Bloom Foundation. and was supported by AtlantECO (project number: 862923) as well as TipESM and ClimTIP, which are both funded by the European Union, Views and opinions expressed are however those of the author (s) only and do not necessarily reflect those of the European Union or the European Climate, Infrastructure and Environment Executive Agency (CINEA). Neither the European Union nor the granting authority can be held responsible for them. We also thank the CSCS Swiss National Supercomputing Centre for computing resources and two reviewers for their helpful comments.

References

- Arias-Ortiz, A., Serrano, O., Masqué, P., Lavery, P., Mueller, U., Kendrick, G., et al. (2018). A marine heatwave drives massive losses from the world's largest seagrass carbon stocks. *Nature Climate Change*, 8(4), 338–344. https://doi.org/10.1038/s41558-018-0096-y
- Atlas, R., Hoffman, R. N., Ardizzone, J., Leidner, M., Jusem, J. C., Smit, D. K., & Gombos, D. (2011). Cross-calibrated, multiplatform ocean surface wind velocity product for meteorological and oceanographic applications. *Journal of Climate*, 92(2), 157–174. https://doi.org/10.1029/20191C015367
- Bakker, D. C. E., Pfeil, B., Landa, C. S., Metzl, N., O'Brien, K. M., Olsen, A., et al. (2016). A multi-decade record of high-quality fCO₂ data in version 3 of the surface ocean CO₂ atlas (SOCAT). Earth System Science Data, 8(2), 383–413. https://doi.org/10.5194/essd-8-383-2016
- Bian, C., Jing, Z., Wang, H., Wu, L., Chen, Z., Gan, B., & Yang, H. (2023). Oceanic mesoscale eddies as crucial drivers of global marine heatwaves. *Nature Communications*, 14(1), 2970. https://doi.org/10.1038/s41467-023-38811-z
- Boyer, T. P., García, H. E., Locarnini, R. A., Zweng, M. M., Mishonov, A. V., Reagan, J. R., et al. (2018). World Ocean Atlas 2018. Volume 4: Dissolved inorganic nutrients (phosphate, nitrate and nitrate+nitrite, silicate). NOAA National Centers for Environmental Information. Dataset. Retrieved from https://www.ncei.noaa.gov/archive/accession/NCEI-WOA18
- Burger, F. A., & Frölicher, T. L. (2023). Drivers of Surface Ocean acidity extremes in an Earth system model. *Global Biogeochemical Cycles*, 37(9), e2023GB007785. https://doi.org/10.1029/2023GB007785
- Burger, F. A., Terhaar, J., & Frölicher, T. L. (2022). Compound marine heatwaves and ocean acidity extremes. *Nature Communications*, 13(4722), 4722. https://doi.org/10.1038/s41467-022-32120-7
- Carter, B. R., Feely, R. A., Williams, N. L., Dickson, A. G., Fong, M. B., & Takeshita, Y. (2018). Updated methods for global locally interpolated estimation of alkalinity, pH, and nitrate. Limnology and Oceanography: Methods, 16(2), 119–131. https://doi.org/10.1002/lom3.10232
- Chau, T. T. T., Gehlen, M., & Chevallier, F. (2022). A seamless ensemble-based reconstruction of surface ocean pCO₂ and air-sea CO₂ fluxes over the global coastal and open oceans. *Biogeosciences*, 19(4), 1087–1109. https://doi.org/10.5194/bg-19-1087-2022
- Cheung, W. W. L., & Frölicher, T. L. (2020). Marine heatwaves exacerbate climate change impacts for fsheries in the northeast Pacific. Scientific Reports, 10(1), 6678. https://doi.org/10.1038/s41598-020-63650-z
- Cheung, W. W. L., Frölicher, T. L., Lam, V. W. Y., Oyinlola, M. A., Reygondeau, G., Sumaila, U. R., et al. (2021). Marine high temperature extremes amplify the impacts of climate change on fish and fisheries. *Science Advances*, 7(40). https://doi.org/10.1126/sciadv.abh0895
- Ciais, P., Viovy, N., Reichstein, M., Seufert, G., Matteucci, G., Allard, V., et al. (2005). Europe-wide reduction in primary productivity caused by the heat and drought in 2003. *Nature*, 437(7058), 529–533. https://doi.org/10.1038/nature03972
- Collins, M., Sutherland, M., Bouwer, L., Cheong, S.-M., Frölicher, T., Jacot Des Combes, H., et al. (2019). Extremes, abrupt changes and managing risk. In *IPCC special report on the ocean and cryosphere in a changing climate (Tech. Rep.)*. University Press.
- Denvil-Sommer, A., Gehlen, M., Vrac, M., & Mejia, C. (2019). LSCE-FFNN-v1: A two-step neural network model for the reconstruction of surface ocean pCO₂ over the global ocean. Geoscientific Model Development, 12(5), 2091–2105. https://doi.org/10.5194/gmd-12-2091-2019
- Doney, S. C., Lima, I., Feely, R. A., Glover, D. M., Lindsay, K., Mahowald, N., et al. (2009). Mechanisms governing interannual variability in upper-ocean inorganic carbon system and air-sea co2CO₂ fluxes: Physical climate and atmospheric dust. *Deep Sea Research Part II: Topical Studies in Oceanography*, 56(8–10), 640–655. https://doi.org/10.1016/j.dsr2.2008.12.006
- Dong, Y., Bakker, D. C. E., & Landschützer, P. (2024). Accuracy of ocean CO₂ uptake estimates at a risk by a reduction in the data collection. Geophysical Research Letters, 51(9), e2024GL108502. https://doi.org/10.1029/2024GL108502
- Duke, P. J., Hamme, R. C., Ianson, D., Landschützer, P., Ahmed, M. M. M., Swart, N. C., & Covert, P. A. (2023). Estimating marine carbon uptake in the northeast Pacific using a neural network approach. *Biogeosciences*, 20, 3919–3941. https://doi.org/10.5194/egusphere-2023-870
- Edwing, K., Wu, Z., Lu, W., Li, X., Cai, W.-J., & Yan, X.-H. (2024). Impact of marine heatwaves on air-sea CO₂ flux along the US east coast. Geophysical Research Letters, 51(1). https://doi.org/10.1029/2023GL105363
- Fay, A. R., Gregor, L., Landschützer, P., McKinley, G. A., Gruber, N., Gehlen, M., et al. (2021). Seaflux: Harmonization of air-sea CO₂ fluxes from surface pCO₂ data products using a standardized approach. *Earth System Science Data*, 13(10), 4693–4710. https://doi.org/10.5194/essd-13-4693-2021
- Fay, A. R., & McKinley, G. A. (2017). Correlations of surface ocean pCO₂ to satellite chlorophyll on monthly to interannual timescales. Global Biogeochemical Cycles, 31(3), 436–455. https://doi.org/10.1002/2016GB005563
- Frank, D., Reichstein, M., Bahn, M., Thonicke, K., Frank, D., Mahecha, M. D., et al. (2015). Effects of climate extremes on the terrestrial carbon cycle: Concepts, processes and potential future impacts. *Global Change Biology*, 21(8), 2861–2880. https://doi.org/10.1111/gcb.12916
- Friedlingstein, P., O'Sullivan, M., Jones, M. W., Andrew, R. M., Bakker, D. C. E., Hauck, J., et al. (2023). Global carbon budget 2023. Earth System Science Data, 15(12), 5301–5369. https://doi.org/10.5194/essd-15-5301-2023
- Frölicher, T. L., Fischer, E. M., & Gruber, N. (2018). Marine heatwaves under global warming. *Nature*, 560(7718), 360–364. https://doi.org/10.1038/s41586-018-0383-9
- Frölicher, T. L., & Laufkötter, C. (2018). Emerging risks from marine heat waves. Nature Communications, 9(1), 650. https://doi.org/10.1038/s41467-018-03163-6
- Garcia, H. E., Weathers, C. R., Paver, K., Smolyar, I., Boyer, T. P., Locarnini, R. A., et al. (2019). World Ocean Atlas 2018, volume 4: Dissolved inorganic nutrients (phosphate, nitrate and nitrate+nitrite, silicate). A. Mishonov Technical Ed.; NOAA Atlas NESDIS 84.
- Gattuso, J.-P., Magnan, A., Billé, R., Cheung, W. W. L., Howes, E. L., Joos, F., et al. (2015). Contrasting futures for ocean and society from different anthropogenic CO₂ emissions scenarios. *Science*, 349(6243), aac4722. https://doi.org/10.1126/science.aac4722

LI ET AL. 10 of 12

- Good, S. A., Martin, M. J., & Rayner, N. A. (2013). EN4: Quality controlled ocean temperature and salinity profiles and monthly objective analyses with uncertainty estimates. *Journal of Geophysical Research: Oceans*, 118(12), 6704–6716. https://doi.org/10.1002/2013JC009067
- Gray, A. R., Johnson, K. S., Bushinsky, S. M., Riser, S. C., Russell, J. L., Talley, L. D., et al. (2018). Autonomous biogeochemical floats detect significant carbon dioxide outgassing in the high-latitude southern ocean. *Geophysical Research Letters*, 45(17), 9049–9057. https://doi.org/10.1029/2018GL078013
- Gregor, L., & Gruber, N. (2021). Oceansoda-ethz: A global gridded data set of the surface ocean carbonate system for seasonal to decadal studies of ocean acidification. Earth System Science Data, 13(2), 777–808. https://doi.org/10.5194/essd-13-777-2021
- Gregor, L., Lebehot, A. D., Kok, S., & Scheel Monteiro, P. M. (2019). A comparative assessment of the uncertainties of global surface ocean CO₂ estimates using a machine-learning ensemble (CSIR-ML6 version 2019a) Have we hit the wall? *Geoscientific Model Development*, 12, 5113–5136. https://doi.org/10.5194/gmd-12-5113-2019
- Hasselmann, K. (1976). Stochastic climate models part i. theory. Tellus, 28(6), 473-485. https://doi.org/10.1111/j.2153-3490.1976.tb00696.x
- Hersbach, H., Bell, B., Berrisford, P., Hirahara, S., Horányi, A., Muñoz-Sabater, J., et al. (2020). The ERA5 global reanalysis. *Quarterly Journal of the Royal Meteorological Society*, 146(730), 1999–2049. https://doi.org/10.1002/qj.3803
- Hobday, A. J., Alexander, L. V., Perkins, S. E., Smale, D. A., Straub, S. C., Oliver, E. C., et al. (2016). A hierarchical approach to defining marine heatwaves. *Progress in Oceanography*, 141, 227–238. https://doi.org/10.1016/j.pocean.2015.12.014
- Holbrook, N., Scannell, H. A., Gupta, A. S., Benthuysen, J. A., Feng, M., Oliver, E. C. J., et al. (2019). A global assessment of marine heatwaves and their drivers. *Nature Communications*, 10(1), 2624. https://doi.org/10.1038/s41467-019-10206-z
- Huang, B., Liu, C., Banzon, V., Freeman, E., Graham, G., Hankins, B., et al. (2021). Improvements of the daily optimum interpolation sea surface temperature (DOISST), version 2.1. *Journal of Climate*, 34(8), 2923–2939. https://doi.org/10.1175/JCLI-D-20-0166.1
- Hughes, T., Kerry, J., Alvarez-Noriega, M., Álvarez Romero, J., Anderson, K., Baird, A., et al. (2017). Global warming and recurrent mass bleaching of corals. *Nature*. 543(7645), 373–377. https://doi.org/10.1038/nature21707
- Humphreys, M. P., Lewis, E. R., Sharp, J. D., & Pierrot, D. (2022). PyCO2SYS v1.8: Marine carbonate system calculations in Python. Geoscientific Model Development, 15(1), 15–43. https://doi.org/10.5194/gmd-15-15-2022
- lida, Y., Takatani, Y., Kojima, A., & Ishii, M. (2020). Global trends of ocean CO₂ sink and ocean acidifcation: An observation-based reconstruction of surface ocean inorganic carbon variables. *Journal of Oceanography*, 77(2), 323–358. https://doi.org/10.1007/s10872-020-00571-5
- IPCC. (2021). Summary for policymakers. In V. Masson-Delmotte, P. Zhai, A. Pirani, S. L. Connors, C. Péan, S. Berger, et al. (Eds.), Climate change 2021: The physical science basis. Contribution of working group I to the sixth assessment report of the intergovernmental panel on climate change (pp. 3–32). Cambridge University Press. https://doi.org/10.1017/9781009157896.001
- Joos, F., Plattner, G.-K., Stocker, T. F., Marchal, O., & Schmittner, A. (1999). Global warming and marine carbon cycle feedbacks on future atmospheric CO₂. Science, 284(5413), 464–467. https://doi.org/10.1126/science.284.5413.464
- Kalnay, E., Kanamitsu, M., Kistler, R., Collins, W., Deaven, D., Gandin, L., et al. (1996). The NCEP/NCAR 40-year reanalysis project. Bulletin of the American Meteorological Society, 77(2), 437–472. https://doi.org/10.1175/1520-0477(1996)077(0437:TNYRP)2.0.CO
- Kanamitsu, M., Ebisuzaki, W., Woollen, J., Yang, S.-K., Hnilo, J. J., Fiorino, M., & Potter, G. L. (2002). NCEP-DOE AMIP-II reanalysis. Bulletin of the American Meteorological Society, 83(11), 1631–1644. https://doi.org/10.1175/BAMS-83-11-1631
- Ke, P., Ciais, P., Sitch, S., Li, W., Bastos, A., Liu, Z., et al. (2024). Low latency carbon budget analysis reveals a large decline of the land carbon sink in 2023. Retrieved from https://arxiv.org/abs/2407.12447
- Kobayashi, S., Ota, Y., Harada, Y., Ebita, A., Moriya, M., Onoda, H., et al. (2015). The JRA-55 reanalysis: General specifications and basic characteristics. *Journal of the Meteorological Society of Japan*, 93(1), 5–48. https://doi.org/10.2151/jmsj.2015-001
- Landschützer, P., Gruber, N., & Bakker, D. C. E. (2016). Decadal variations and trends of the global ocean carbon sink. *Global Biogeochemical Cycles*, 30(10), 1396–1417. https://doi.org/10.1002/2015GB005359
- Landschützer, P., Gruber, N., & Bakker, D. C. E. (2020). An observation-based global monthly gridded sea surface pCO₂ product from 1982 onward and its monthly climatology. NOAA National Centers for Environmental Information.
- Landschützer, P., Gruber, N., Bakker, D. C. E., & Schuster, U. (2014). Recent variability of the global ocean carbon sink. *Global Biogeochemical Cycles*, 28(9), 927–949. https://doi.org/10.1002/2014GB004853
- Le Grix, N., Zscheischler, J., Laufkötter, C., Rousseaux, C. S., & Frölicher, T. L. (2021). Compound high-temperature and low-chlorophyll extremes in the ocean over the satellite period. *Biogeosciences*, 18(6), 2119–2137. https://doi.org/10.5194/bg-18-2119-2021
- Li, C., & Burger, F. (2024). Analysis code for the publication "Observed regional impacts of marine heatwaves on sea-air CO₂ exchange" [Software]. Zenodo. https://doi.org/10.5281/zenodo.14152716
- Lovenduski, N. S., Gruber, N., Doney, S. C., & Lima, I. D. (2007). Enhanced co2CO₂ outgassing in the southern ocean from a positive phase of the southern annular mode. *Global Biogeochemical Cycles*, 21(2), GB2026. https://doi.org/10.1029/2006GB002900
- Merchant, C. J., Owen, E., Bulgin, C. E., Block, T., Corlett, G. K., Fiedler, E., et al. (2019). Satellite-based time-series of sea-surface temperature since 1981 for climate applications. *Scientific Data*, 6(1), 223. https://doi.org/10.1038/s41597-019-0236-x
- Mignot, A., von Schuckmann, K., Landschützer, P., Gasparin, F., van Gennip, S., Perruche, C., et al. (2022). Decrease in air-sea CO₂ fluxes caused by persistent marine heatwaves. *Nature Communications*, 13(1), 4300. https://doi.org/10.1038/s41467-022-31983-0
- Oliver, E. C. J., Benthuysen, J. A., Darmaraki, S., Donat, M. G., Hobday, A. J., Holbrook, N. J., et al. (2021). Marine heatwaves. *Annual Review of Marine Science*, 13(1), 313–342. https://doi.org/10.1146/annurev-marine-032720-095144
- Oliver, E. C. J., Burrows, M. T., Donat, M. G., Sen Gupta, A., Alexander, L. V., Perkins-Kirkpatrick, S. E., et al. (2019). Projected marine heatwaves in the 21st century and the potential for ecological impact. Frontiers in Marine Science, 6. https://doi.org/10.3389/fmars.2019.00734
- Oliver, E. C. J., Donat, M. G., Burrows, M. T., Moore, P. J., Smale, D. A., Alexander, L. V., et al. (2018). Longer and more frequent marine heatwaves over the past century. *Nature Communications*, 9, 1–12. https://doi.org/10.1038/s41467-018-03732-9
- Orr, J. C., & Epitalon, J.-M. (2015). Improved routines to model the ocean carbonate system: Mocsy 2.0. Geoscientific Model Development, 8(3), 485–499. https://doi.org/10.5194/gmd-8-485-2015
- Pearce, A. F., & Feng, M. (2013). The rise and fall of the "marine heat wave" off western Australia during the summer of 2010/2011. *Journal of Marine Systems*, 111–112, 139–156. https://doi.org/10.1016/j.jmarsys.2012.10.009
- Reichstein, M., Bahn, M., Philippe Ciais and, D. F., Mahecha, M. D., Seneviratne, S. I., Zscheischler, J., et al. (2013). Climate extremes and the carbon cycle. *Nature*, 500(500), 287–295. https://doi.org/10.1038/nature12350
- Rödenbeck, C., Keeling, R. F., Bakker, D. C. E., Metzl, N., Olsen, A., Sabine, C., & Heimann, M. (2013). Global surface-ocean pCO₂ and sea–air CO₂ flux variability from an observation-driven ocean mixed-layer scheme. *Ocean Science*, 9(2), 193–216. https://doi.org/10.5194/os-9-193-
- Smale, D. A., Wernberg, T., Oliver, E. C. J., Thomsen, M., Harvey, B. P., Straub, S. C., et al. (2019). Marine heatwaves threaten global biodiversity and the provision of ecosystem services. *Nature Climate Change*, 9(4), 306–312. https://doi.org/10.1038/s41558-019-0412-1

LI ET AL. 11 of 12

- Takahashi, T., Olafsson, J., Goddard, J. G., Chipman, D. W., & Sutherland, S. C. (1993). Seasonal variation of co2CO₂ and nutrients in the high-latitude surface oceans: A comparative study. *Global Biogeochemical Cycles*, 7(4), 843–878. https://doi.org/10.1029/93GB02263
- Takahashi, T., Sutherland, S. C., Sweeney, C., Poisson, A., Metzl, N., Tilbrook, B., et al. (2002). Global sea-air CO₂ flux based on climatological surface ocean pCO₂, and seasonal biological and temperature effects. *Deep Sea Research Part II: Topical Studies in Oceanography*, 49(9), 1601–1622. https://doi.org/10.1016/S0967-0645(02)00003-6
- Vogt, L., Burger, F. A., Griffies, S. M., & Frölicher, T. L. (2022). Local drivers of marine heatwaves: A global analysis with an Earth system model. Frontiers in Climate, 4. https://doi.org/10.3389/fclim.2022.847995
- Wanninkhof, R. (1992). Relationship between wind speed and gas exchange over the ocean revisited. *Journal of Geophysical Research*, 97(C5), 7373–7382. https://doi.org/10.4319/lom.2014.12.351
- Wilks, D. S. (2019). Statistical methods in the atmospheric sciences. In *Statistical methods in the atmospheric sciences* (4th ed., pp. 771–805). Elsevier. https://doi.org/10.1016/B978-0-12-815823-4.09992-2
- Zeng, J., Nojiri, Y., Landschützer, P., Telszewski, M., & Nakaoka, S.-i. (2014). A global surface ocean fCO₂ climatology based on a feed-forward neural network. *Journal of Atmospheric and Oceanic Technology*, 31(8), 1838–1849. https://doi.org/10.1175/JTECH-D-13-00137.1
- Zscheischler, J., & Seneviratne, S. I. (2017). Dependence of drivers affects risks associated with compound events. *Science Advances*, 3(6), e1700263. https://doi.org/10.1126/sciadv.1700263

LI ET AL. 12 of 12